Review of Scientific Instruments

Optimal deformation procedure for hybrid adaptive x-ray mirror based on mechanical and piezo-driven bending system

Cite as: Rev. Sci. Instrum. **92**, 123706 (2021); https://doi.org/10.1063/5.0070465
Submitted: 07 September 2021 • Accepted: 19 November 2021 • Published Online: 28 December 2021

Takato Inoue, Yuka Nishioka, Satoshi Matsuyama, et al.

Review of Scientific Instruments ARTICLE scitation.org/journal/rsi

Optimal deformation procedure for hybrid adaptive x-ray mirror based on mechanical and piezo-driven bending system

Cite as: Rev. Sci. Instrum. 92, 123706 (2021); doi: 10.1063/5.0070465
Submitted: 7 September 2021 • Accepted: 19 November 2021 •
Published Online: 28 December 2021

Takato Inoue,[1,a] Yuka Nishioka,[1] Satoshi Matsuyama,[1,2] Junki Sonoyama,[3] Kazuteru Akiyama,[3] Hiroki Nakamori,[4] Yoshio Ichii,[4] Yasuhisa Sano,[1] Xianbo Shi,[5] Deming Shu,[5] Max D. Wyman,[5] Ross Harder,[5] Yoshiki Kohmura,[6] Makina Yabashi,[6,7] Lahsen Assoufid,[5] Tetsuya Ishikawa,[6] and Kazuto Yamauchi[1,8]

AFFILIATIONS

[1] Department of Precision Science and Technology, Graduate School of Engineering, Osaka University, 2-1 Yamada-oka, Suita, Osaka 565-0871, Japan
[2] Department of Materials Physics, Graduate School of Engineering, Nagoya University, Furo-cho, Chikusa-ku, Nagoya, Aichi 464-8603, Japan
[3] TOYAMA, 3816-1 Kishi, Yamakita-machi, Ashigarakami-gun, Kanagawa 258-0112, Japan
[4] JTEC Corporation, 2-5-38, Saito-Yamabuki, Ibaraki, Osaka 567-0086, Japan
[5] Advanced Photon Source, Argonne National Laboratory, 9700 South Cass Avenue, Argonne, Illinois 60439, USA
[6] RIKEN SPring-8 Center, 1-1-1 Kouto, Sayo-cho, Sayo-gun, Hyogo 679-5148, Japan
[7] Japan Synchrotron Radiation Research Institute, 1-1-1 Kouto, Sayo-cho, Sayo-gun, Hyogo 679-5198, Japan
[8] Center for Ultra-Precision Science and Technology, Graduate School of Engineering, Osaka University, 2-1 Yamada-oka, Suita, Osaka 565-0871, Japan

[a] **Author to whom correspondence should be addressed:** t.inoue@up.prec.eng.osaka-u.ac.jp

ABSTRACT

A hybrid deformable x-ray mirror consisting of a mechanical bender and a bimorph deformable mirror has been developed to realize adaptive optical systems, such as zoom condenser optics, for synchrotron-radiation-based x-ray microscopy. In the developed system, both bending mechanisms comprehensively contribute to the formation of the target mirror shape and can narrow the role of piezoelectric actuators, thereby enabling a more stable operation. In this study, the behavior of the bimorph mirror under the clamped condition was investigated, and the sharing of the deformation amount for each bending mechanism was optimized to minimize the amplitude of the voltage distribution of the bimorph mirror.

I. INTRODUCTION

Hard x-ray microscopy can visualize the internal structures, elemental maps, and chemical bonding states of electronic devices, biological tissues, and advanced materials. The sensitivity and spatial resolution of these results are strongly dependent on the focusing optics. In the hard x-ray regime, several types of optics—such as refractive lenses,[1,2] zone plates,[3] mirrors,[4–6] and multilayer Laue lenses[7]—are available and have been appropriately selected and utilized. Among these, mirrors are superior owing to their high throughput, low chromatic aberration, and excellent radiation hardness. However, the precision required in their fabrication is extremely high; roughness or shape errors, even in the nanometer range or less, could degrade the mirror focusing characteristics, leading to the broadening of the spot size and a reduction in peak intensity. Over the past two decades, precision-fabrication methods[8–11] and surface-testing methods[12–16] have been developed to produce ultraprecise mirrors in the hard x-ray regime. These mirrors have led to advances in x-ray microscopy and analysis methods. However, the optical parameters of the mirror devices were fixed depending on the

usage. The focus size is determined by diffraction theory with shape parameters to preserve beam coherency.

Newly established synchrotron radiation x-ray sources, such as x-ray free-electron lasers (XFELs) and upgraded third-generation synchrotron radiation sources, would significantly benefit from the availability of advanced adaptive mirror devices to freely and accurately alter the optical parameters to match the sample conditions. For example, the high throughput of upgraded third-generation synchrotron sources enables multiple analyses within a limited beam time; thus, it is necessary to adapt the focus size for each analysis appropriately. In XFELs, changing the beam size is considerably vital for the irradiation of specimens of various sizes owing to the small number of beamlines. Recently, mirror devices with adaptivity have been developed to meet these requirements.

Adaptive optical systems have also been proposed to change the focus size with a diffraction-limited performance by using precision bimorph mirrors, which can be deformed with piezoelectric actuators built into the mirror substrate.[17–21] Moreover, a hybrid deformable mirror comprising a precision mechanical bender and a bimorph deformable mirror was recently proposed, in which the demerits of the bimorph mirror, such as drifts over time and junction effects,[18] are effectively compensated by the mechanical bender, thereby enabling stable operation.[22–24]

In the hybrid deformable mirror, the target shape can be generated comprehensively by mechanically applying moments at both ends and distributing the moments induced by piezoelectric actuators on the bimorph mirror. Practically, each of the two bending mechanisms can generate deformation profiles up to third-order polynomials, leading to various combinations of the mechanical bender and bimorph mirror contributions. For a stable operation of the hybrid deformable mirror, the role of the bimorph mirror should be minimized such that the demerits of the drifts and junction effects are reduced. In this study, we proposed an optimal operation method supported by experimental confirmation and investigated the characteristics of bimorph mirror behavior under clamped conditions using a finite-element method (FEM) simulation. We found that, to reduce the applied voltage to the bimorph mirror, the residual error to be corrected by the bimorph mirror should not be minimized but should instead be slightly modified to be larger by the mechanical bender.

II. HYBRID DEFORMABLE MIRROR

Figure 1(a) presents the design of the developed hybrid deformable mirror, which includes a mechanical bender and piezoelectric bimorph mirror. Table I lists the parameters of the developed system. The bimorph mirror was initially flat with a length, width, and thickness of 400, 30, and 15 mm, respectively. Piezoelectric plate actuators, composed of lead zirconate titanate (PZT), are glued on each side wall in two lines along the upper and lower surfaces. The dimensions of the electrodes deposited on the upper surface of the piezoelectric plates are 15.9×5 mm^2, with an interval of 0.8 mm, and each line consisted of 22 electrodes. The substrate could be deformed with a range of short spatial wavelengths down to the size of the four electrodes. Over a shorter range, the shape of the substrate was prepared with sufficient precision using elastic emission machining.[11]

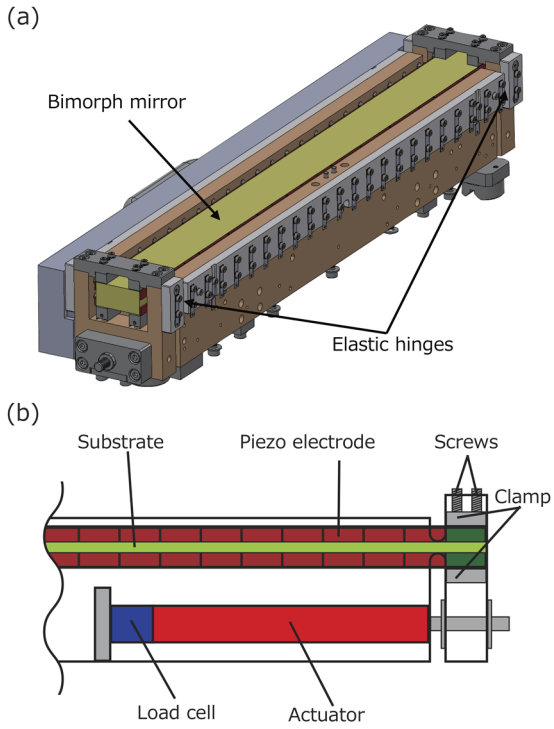

FIG. 1. Schematics of (a) the hybrid deformable mirror and (b) a magnified image of the mirror clamping device (a pair of blocks actuated by screws) and the force generator used to apply the bending moment.

Figure 1(b) shows a cross-sectional view of the mechanical bender. The mirror clamps at both ends were connected to the elastic hinges, enabling rotational freedom. The radius, thickness, and width of hinges were 2.5, 1.0, and 5.0 mm, respectively, ensuring appropriate rigidity. The twisting of the mirror induced by the clamps was evaluated and adjusted with an accuracy better than 10 μrad using the NOM/auto-collimator-based slope profiler of the Advanced Photon Source.[25] To apply a predetermined bending moment, a linear actuator (P-841, Physic Instrument) was employed to push the end of the mirror clamp. The force generated by the linear actuator was monitored using a load cell kinematically mounted on the same axis as the actuator. The other end of the bender has the same structure. The bending moments at both ends can be applied independently, allowing the mirror shape to be controlled up to

TABLE I. Parameters of the piezoelectric bimorph mirror system.

	Mirror substrate	Piezoelectric plate actuator
Material	CLEARCERAM-Z (OHARA INC.)	Lead zirconate titanate (PZT)
Length (mm)	400	400
Width (mm)	30	5
Thickness (mm)	15	1
Young's modulus (GPa)	90	80
Piezoelectric coefficient (m/V)	⋯	-1.35×10^{-10}

third-order polynomials. Finally, the residual shape error is compensated using a bimorph mirror. The mechanical bender can reduce the role of the piezoelectric actuators, thus considerably minimizing the drift and junction effects, which are the most significant problems when using piezoelectric actuators.

III. FINITE-ELEMENT METHOD SIMULATION

To understand the shape-correction characteristics of the bimorph mirror under the clamped condition, we investigated the response functions of the mirror shape formed by piezoelectric actuators by conducting an FEM simulation. The results are discussed in comparison with the free-standing condition. Figure 2(a) demonstrates the calculated response functions of the bimorph mirror under free-standing conditions. The applied voltage was 250 V in all cases. Figure 2(b) shows the curvature distributions derived from Fig. 2(a). As expected, only the curvature of the active electrode changed. Figure 3(a) illustrates the response functions calculated when both ends are clamped. Compared to Fig. 2(a),

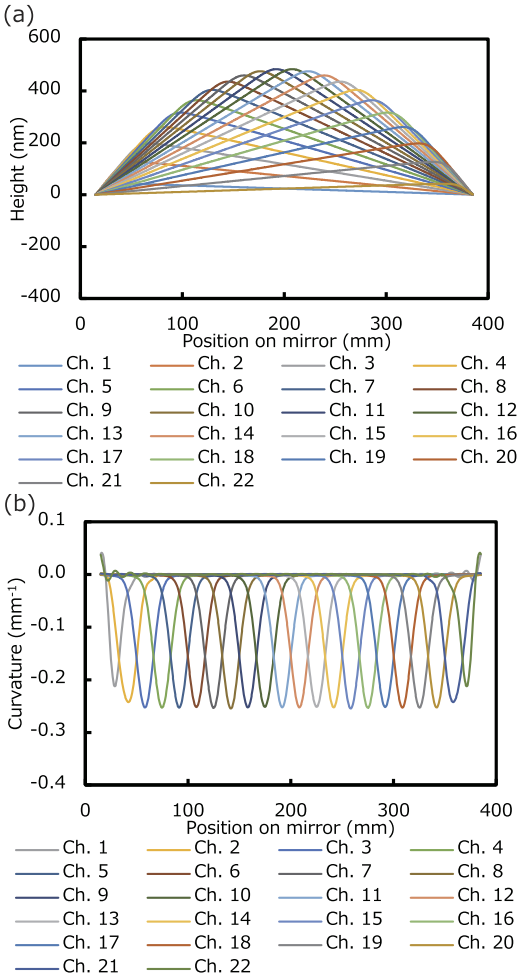

FIG. 2. FEM calculation results of (a) response function and (b) curvature distribution under the free-standing condition when 250 V was applied to each channel of the piezoelectric actuators.

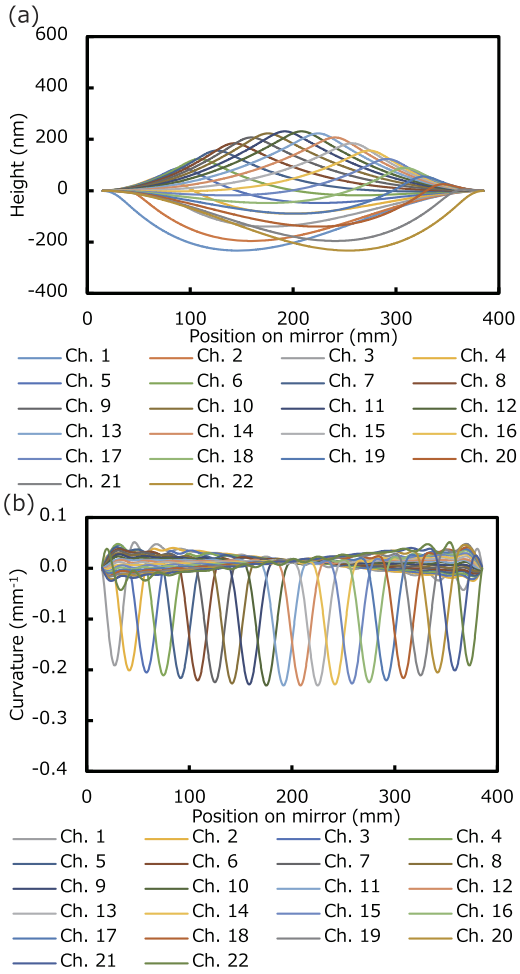

FIG. 3. FEM calculation results of (a) response function and (b) curvature distribution under the clamped condition when 250 V was applied to each channel of the piezoelectric actuators.

bending is distributed over the entire surface of the mirror and becomes concave in an area away from the active electrode. The concave shape becomes steeper as the electrode closer to the clamper is activated. Figure 3(b) presents the curvature distributions derived from Fig. 3(a). The shape-correction characteristics of the clamped mirror are significantly different from those of the free-standing mirror and are more complex because of the reaction moment at the clamp.

Figure 4(a) presents the curvature distributions generated under the free-standing and clamped conditions when 250 V was applied to all electrodes. In both cases, constant curvatures were generated over the effective surface of the mirror, each of which indicates the deformation of a parabolic sag. Particularly, in the free-standing case, the parabolic sag was easily evident, and the mirror shape y can be expressed as follows:

$$y = \alpha M_a x^2, \tag{1}$$

where x is the position on the mirror, α is a constant, and M_a is the bending moment induced by the piezoelectric actuator. In

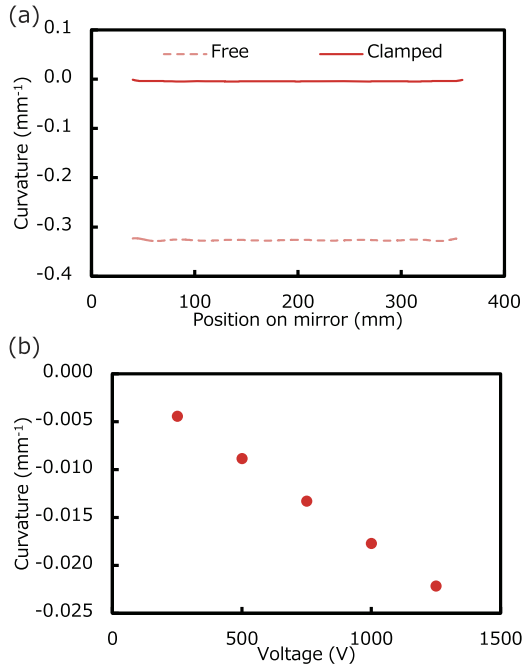

FIG. 4. (a) Comparison of curvature distributions between clamped and free-standing cases when 250 V was applied to all electrodes. (b) Relationship between applied voltages and curvatures under the clamped condition.

contrast, when both ends of the mirror are clamped and piezoelectric actuators apply constant moments over the mirror's full length, the moment distribution should be compensated to be zero by the reactive moment M_r, induced at both ends assuming perfect clamping conditions. In the mirror developed in this study, the rigidity of the thin screws necessary to push the clamping blocks allows a slight parabolic sag deformation, and the mirror shape can be given by

$$y = \alpha(M_a - M_r)x^2. \quad (2)$$

Meanwhile, the amplitude in the clamped case was considerably smaller than that in the free-standing case. Figure 4(b) shows the relationship between the curvature and voltage applied to all the electrodes under the clamped condition. The curvatures generated by the bending moment $(M_a - M_r)$ change proportionally to the applied voltage.

This is equivalent to a deformation induced by the mechanical bender with the same moments at both ends, implying that there are many solutions to generate the required shape and that the optimal solution should be used to reduce the role of piezoelectric actuators.

We investigated the shape-generation characteristics using the target shape shown in Fig. 5(a). Table II lists the shape parameters. Error 1 in Fig. 5(a) indicates the minimal shape error after the parabolic sag and cubic function are completely removed by the mechanical bender. Figure 5(b) displays the final shape error after correction by the bimorph mirror. Under both conditions, the shape errors were reduced to less than 1 nm peak-to-valley (PV). However, as shown in Fig. 5(c), the required voltage becomes significantly higher in the clamped case, for example, higher than 1000 V, whereas it is within a few hundred volts in the free-standing case.

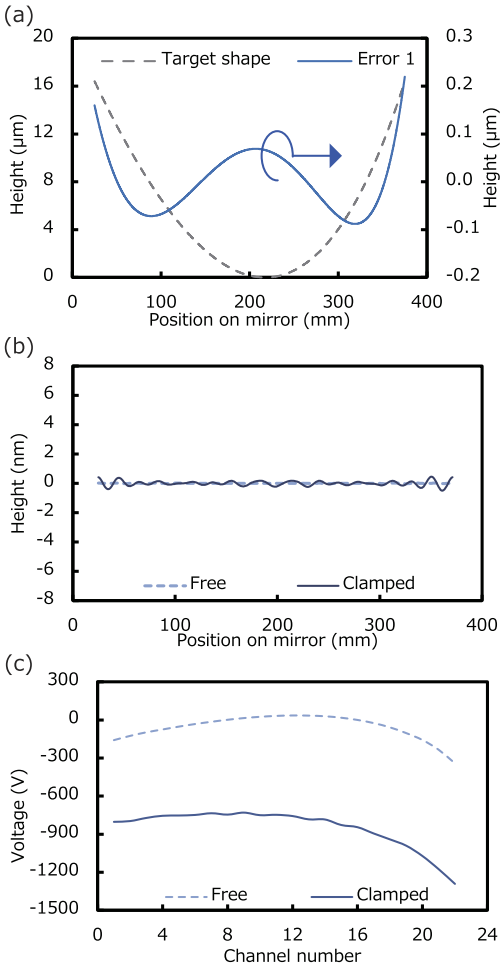

FIG. 5. (a) Target ellipse (Target shape) and minimum shape error to be obtained by the mechanical bender (Error 1). (b) Final shape errors in clamped (Clamped) and free-standing (Free) cases after correction by piezoelectric actuators on the bimorph mirror. (c) Required voltage distribution to correct Error 1 of (a) under clamped (Clamped) and free-standing (Free) conditions.

This can be attributed to the characteristic response functions of the clamped mirror. Thus, clamping has a significant adverse effect on shape generation.

If a free-standing bimorph mirror without a mechanical bender is used, the bimorph mirror must generate the target shape entirely with parabolic sag and cubic function components, leading to a considerably higher amplitude of the voltage distribution. To reduce the

TABLE II. Parameters of the ellipse figure.

a[a] (m)	22.23
b[a] (mm)	40.05
Grazing incidence angle[b] (mrad)	0.90
Focal length[c] (mm)	450

[a] Ellipse: $x^2/a^2 + y^2/b^2 = 1$.
[b] Averaged over the whole area.
[c] At the center of the mirror.

amplitude under the clamped condition, using the characteristics shown in Fig. 4, the voltage distribution could be shifted by intentionally adding a slight parabolic sag with the mechanical bender. In addition, by adding a slight cubic function, the voltage distribution could be linearly inclined. These modifications before the final correction could remove the linear function component from the temporal voltage distribution, leading to a lower amplitude.

Error 1 (the shape error) depicted in Fig. 6(a) is the same as that shown in Fig. 5(a). The voltage distribution used to remove this error is denoted as Error 1 (Clamped) in Fig. 6(b), which has the same profile as that shown in Fig. 5(c) and is unacceptably high. Error 2 in Fig. 6(a) is an appropriately modified shape error in which the mechanical bender intentionally leaves an additional shape error to reduce the amplitude of the voltage distribution at the final shape correction. Error 2 (Clamped) shown in Fig. 6(b) is the required voltage distribution to correct Error 2, and it leads to a much lower amplitude than Error 1 (Clamped) as expected and is closer to Error 1 (Free). This result depends on the property shown in Fig. 4, indicating that the amplitude of the voltage distribution can be suitably minimized by tweaking the mechanical bending.

We can summarize the optimized shape-generation flow as follows: Once the target shape is provided, the higher-order components are estimated by excluding those of the parabolic sag and cubic function; the voltage distribution for the bimorph mirror is calculated using the minimum square method. Then, using the property shown in Fig. 4(b) which can be estimated from the practical response functions of the piezoelectric actuators obtained on-site, the target shape for the bimorph mirror is modified by leaving an additional parabolic sag and/or cubic function by the mechanical bender, leading to a shift and inclination of the voltage distribution to minimize the amplitude.

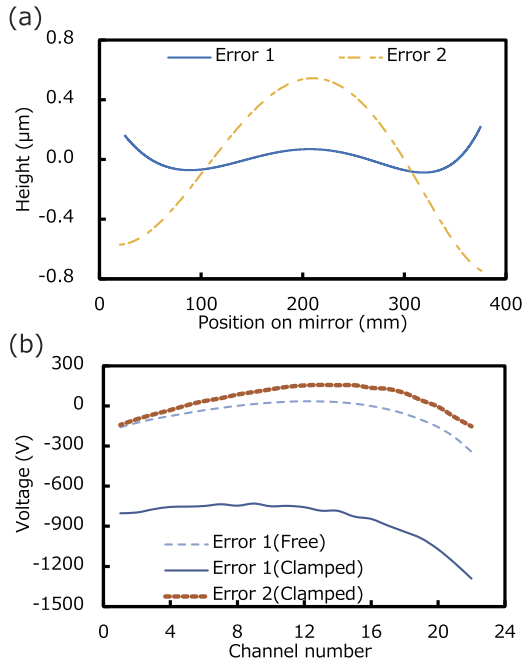

FIG. 6. (a) Error 1 represents the minimum shape error achievable using the mechanical bender, which is the same as that shown in Fig. 5(a). Error 2 is a shape error in which a proper parabolic sag is added to Error 1. (b) Required voltage distribution to correct Error 1 of (a) under the clamped [Error 1 (Clamped)] and free-standing [Error 1 (Free)] conditions and Error 2 of (a) under the clamped [Error 2 (Clamped)] condition.

IV. EXPERIMENTAL SETUP

A one-dimensional focusing experiment using a hybrid deformable mirror was conducted at the experimental hutch 3 of SPring-8 BL29XUL. Figure 7 demonstrates the experimental setup and a photograph of the hybrid deformable mirror. X rays with an energy of 10 keV monochromatized by a Si-111 double-crystal monochromator (DCM) were employed. A transport channel slit placed downstream of the DCM was used as the virtual light source. A slit to define the beam was placed just upstream of the mirror to determine the aperture size of the bimorph mirror. A beam monitor comprising a thin scintillator made of YAG:Ce ceramic, lens, CMOS camera, and gold wire (diameter: 200 μm) was placed at the focal point. The effective mirror length used in the experiment was 350 mm. The optical surface was coated with a platinum thin film (thickness: 100 nm).

The target mirror shape in this demonstration resembled that shown in Fig. 5(a), which was also employed in the above simulations. Pre-shaping can be performed by the response functions of the piezoelectric actuators and mechanical bender, both of which were obtained offline using a coordinate measurement machine.[26] The response functions, obtained by at-wavelength metrology using the pencil beam scanning (PBS) method,[27,28] were used for online shape correction. This method has an angular accuracy of over 10^{-7} rad,

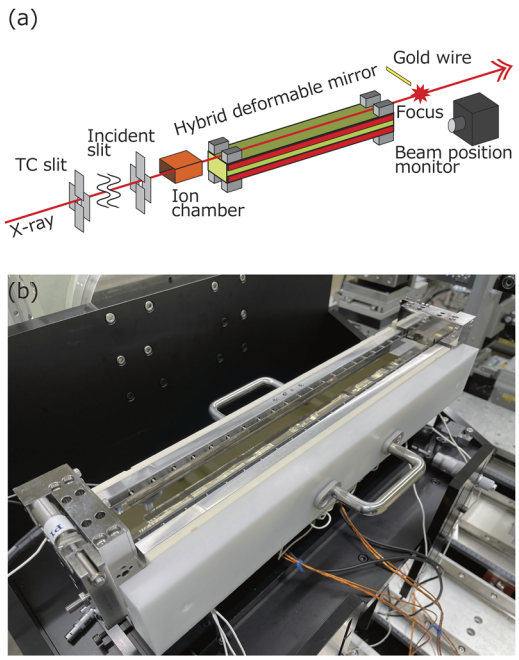

FIG. 7. (a) Experimental setup of one-dimensional x-ray focusing and (b) photograph of the hybrid deformable mirror.

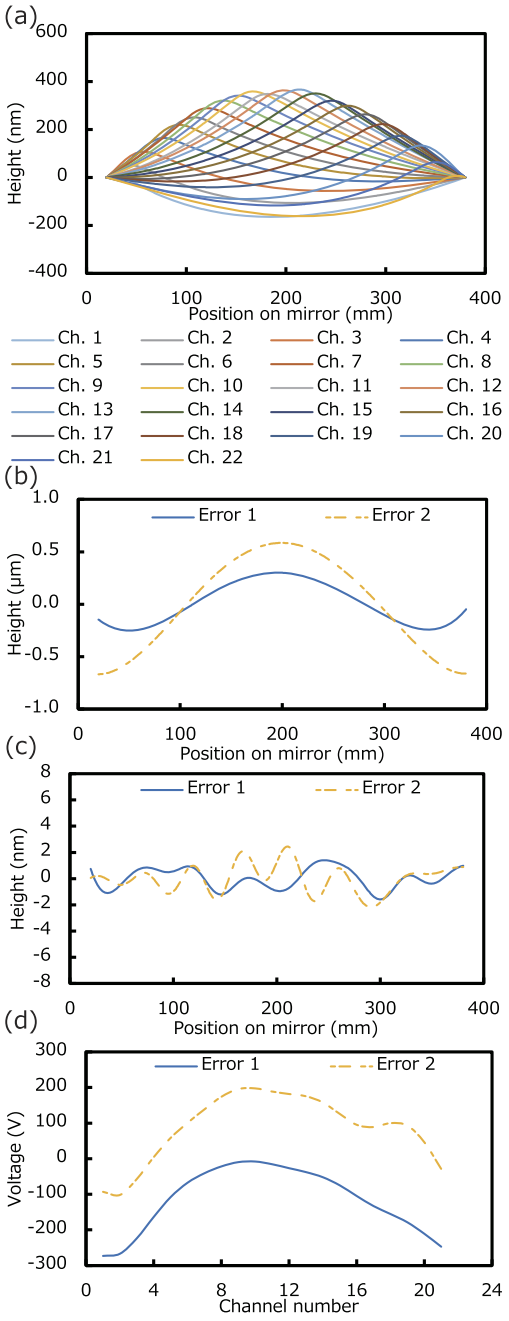

FIG. 8. (a) Response functions of the piezoelectric actuators on the mirror measured by the PBS method at the applied voltage of 250 V. (b) Target shapes for the piezoelectric actuators on the mirror after shape generation by a mechanical bender. Error 1 is the approximately minimum shape error achievable by the mechanical bender; however, it is modified slightly to reduce the amplitude of the voltage distribution applied to the piezoelectric actuators to within ±500 V. Error 2 is a shape error modified to minimize the amplitude of the voltage distribution using the property shown in Fig. 4(b). (c) Shape errors after final correction by the piezoelectric actuators on a bimorph mirror considering Errors 1 and 2 in (b). In both cases, errors in PV nearly satisfy Rayleigh's criterion. (d) Voltage distributions required to correct the shape errors left by the mechanical bender. In the case of Error 2 in (b), the voltage distribution shifts and inclines to reduce the amplitude.

which is sufficient to evaluate the wavefront under diffraction-limited conditions.[29] The shape error profile was obtained by integrating the slope error profile. In the experiment, we first generated a mirror shape using a mechanical bender, the residual shape error of which was set to be correctable by piezoelectric actuators at applied voltages within the −500 to 500 V range, limited by the high-voltage power supply.

V. EXPERIMENTAL RESULTS AND DISCUSSION

Figure 8(a) illustrates the response functions of the piezoelectric actuators measured online by the PBS method at the applied voltage of 250 V. The measured response functions were qualitatively confirmed based on the simulated response functions shown in Fig. 3(a), whereas the imperfection was larger in practice. Figure 8(b) presents the target shapes for the final correction using piezoelectric actuators. The shape error (Error 1) is almost equal to the minimal error used in the simulation after shaping by the mechanical bender, but a little modified to include a small parabolic sag and cubic function to reduce the applied voltage within ±500 V, as mentioned above. Another shape error (Error 2) intentionally includes an additional parabolic sag and cubic function to demonstrate the shifting and inclining of the voltage distribution.

In both cases, the shape errors were corrected online to be less than 4 nm PV, which are slightly larger than those expected by FEM, but were sufficiently small to satisfy the diffraction-limited condition [Fig. 8(c)]. The required voltage distribution for Error 2 has a smaller amplitude than that for Error 1 [Fig. 8(d)]. As discussed previously, the voltage distribution shifted and inclined to a

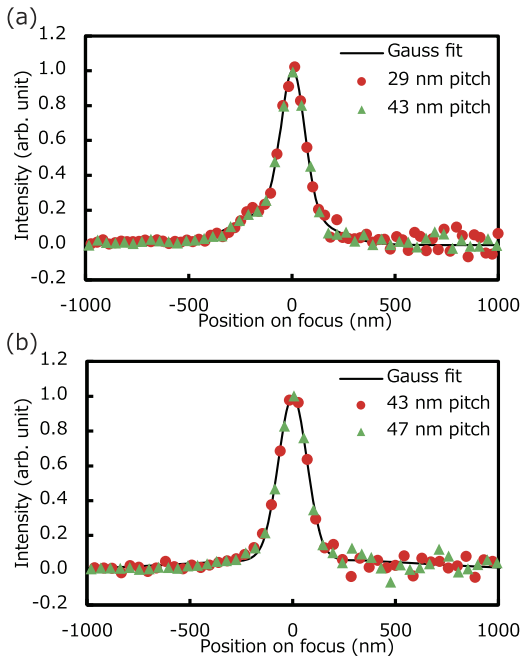

FIG. 9. Intensity profile of focused beam in cases of Errors (a) 1 and (b) 2 of Fig. 8(b). Solid dots represent the values measured twice by a knife-edge scan method with different scan pitches to verify the reproducibility of the results. The solid lines represent those values fitted with double-Gaussian functions.

smaller range. This is a minimization of the final shape error with response functions of not only the piezoelectric actuators but also the mechanical bender with a constraint to minimize the amplitude of the voltage distribution.

For both cases, the focus profiles were measured using a knife-edge scan method, as shown in Fig. 9. The focus sizes in the case of Errors 1 and 2 are 157 and 171 nm for the full width at half maximum, respectively, achieving a nearly diffraction-limited focus size of 141 nm.

VI. CONCLUSIONS

In practice, hybrid deformable mirrors that are inevitably accompanied by some imperfections in clamping, parabolic sag, and cubic functions can be formed using both the mechanical bender and bimorph mirror. Consequently, the mechanical bender and bimorph mirror produced various combinations of contributions. Accordingly, the minimum square method that uses only the shape error and response functions obtained online cannot operate properly. The amplitude of the voltage distribution should be minimized by applying a suitable parabolic sag and cubic function additionally before applying the minimum square method.

The experimental results support the effectiveness of the proposed method for deformation and demonstrate the potential for diffraction-limited performance. Hybrid deformable mirrors with proper operation can attenuate the weaknesses of bimorph mirrors and pave the way for next-generation x-ray microscopy science with zoom condenser optics, which would realize functions of multiple analysis, high flexibility in sample size, and so on. Elucidation of new physical properties of materials and ultrafast dynamics, such as chemical reactions, and determination of the true structure of fragile biological tissues may also be accelerated.

ACKNOWLEDGMENTS

This research was supported by JSPS KAKENHI (Grant Nos. JP16H06358, JP17H01073, JP19J20094, JP20K21146, and JP21H05004) and the CREST project of JST. The work done at the Argonne National Laboratory was supported by the U.S. Department of Energy, Office of Science, Office of Basic Energy Sciences (Contract No. DE-AC02-06CH11357). The authors are grateful to Dr. Takumi Goto, Dr. Jumpei Yamada, Mr. Hiroyuki Yamaguchi, Mr. Kohki Matsumoto, Ms. Nami Nakamura, Mr. Yuto Tanaka, and Mr. Kohei Futamura for their considerable support. They acknowledge the TOYAMA Corporation for helping them develop the mechanical bender system and the JTEC Corporation for helping them with the machining of the mirror substrate. The use of the BL29XUL beamline at SPring-8 was supported by RIKEN.

AUTHOR DECLARATIONS

Conflicts of Interest

The authors have no conflicts to disclose.

DATA AVAILABILITY

The data that support the findings of this study are available from the corresponding author upon reasonable request.

REFERENCES

[1] A. Snigirev, V. Kohn, I. Snigireva, and B. Lengeler, Nature **384**, 49 (1996).
[2] C. G. Schroer, O. Kurapova, J. Patommel, P. Boye, J. Feldkamp, B. Lengeler, M. Burghammer, C. Riekel, L. Vincze, A. Van Der Hart, and M. Küchler, Appl. Phys. Lett. **87**, 124103 (2005).
[3] Y. Suzuki, A. Takeuchi, H. Takano, and H. Takenaka, Jpn. J. Appl. Phys., Part 1 **44**, 1994 (2005).
[4] W. Liu, G. E. Ice, J. Z. Tischler, A. Khounsary, C. Liu, L. Assoufid, and A. T. MacRander, Rev. Sci. Instrum. **76**, 113701 (2005).
[5] H. Mimura, S. Matsuyama, H. Yumoto, H. Hara, K. Yamamura, Y. Sano, M. Shibahara, K. Endo, Y. Mori, Y. Nishlno, K. Tamasaku, M. Yabashi, T. Ishikawa, and K. Yamauchi, Jpn. J. Appl. Phys., Part 2 **44**, L539 (2005).
[6] O. Hignette, P. Cloetens, G. Rostaing, P. Bernard, and C. Morawe, Rev. Sci. Instrum. **76**, 063709 (2005).
[7] H. C. Kang, J. Maser, G. B. Stephenson, C. Liu, R. Conley, A. T. MacRander, and S. Vogt, Phys. Rev. Lett. **96**, 127401 (2006).
[8] O. Hignette, C. Peffen, V. Alvaro, E. Chinchio, and A. K. Freund, Proc. SPIE **4501**, 43 (2001).
[9] M. Idir, L. Huang, N. Bouet, K. Kaznatcheev, M. Vescovi, K. Lauer, R. Conley, K. Rennie, J. Kahn, R. Nethery, and L. Zhou, Rev. Sci. Instrum. **86**, 105120 (2015).
[10] M. Negishi and M. Ando, J. Jpn. Soc. Precis. Eng. **61**, 1393 (1995).
[11] K. Yamauchi, H. Mimura, K. Inagaki, and Y. Mori, Rev. Sci. Instrum. **73**, 4028 (2002).
[12] P. Z. Takacs, S. Qian, and J. Colbert, Proc. SPIE **0749**, 59 (1987).
[13] F. Siewert, T. Noll, T. Schlegel, T. Zeschke, and H. Lammert, AIP Conf. Proc. **705**, 847 (2004).
[14] K. Yamauchi, K. Yamamura, H. Mimura, Y. Sano, A. Saito, K. Ueno, K. Endo, A. Souvorov, M. Yabashi, K. Tamasaku, T. Ishikawa, and Y. Mori, Rev. Sci. Instrum. **74**, 2894 (2003).
[15] H. Mimura, H. Yumoto, S. Matsuyama, K. Yamamura, Y. Sano, K. Ueno, K. Endo, Y. Mori, M. Yabashi, K. Tamasaku, Y. Nishino, T. Ishikawa, and K. Yamauchi, Rev. Sci. Instrum. **76**, 045102 (2005).
[16] F. Siewert, J. Buchheim, S. Boutet, G. J. Williams, P. A. Montanez, J. Krzywinski, and R. Signorato, Opt. Express **20**, 4525 (2012).
[17] J. Susini, D. Labergerie, and L. Zhang, Rev. Sci. Instrum. **66**, 2229 (1995).
[18] R. Signorato, O. Hignette, and J. Goulon, J. Synchrotron Radiat. **5**, 797 (1998).
[19] K. Sawhney, S. Alcock, J. Sutter, S. Berujon, H. Wang, and R. Signorato, J. Phys.: Conf. Ser. **425**, 052026 (2013).
[20] D. J. Merthe, V. V. Yashchuk, K. A. Goldberg, M. Kunz, N. Tamura, W. R. McKinney, N. A. Artemiev, R. S. Celestre, G. Y. Morrison, E. H. Anderson, B. V. Smith, E. E. Domning, S. B. Rekawa, and H. A. Padmore, Opt. Eng. **52**, 033603 (2013).
[21] S. Matsuyama, H. Nakamori, T. Goto, T. Kimura, K. P. Khakurel, Y. Kohmura, Y. Sano, M. Yabashi, T. Ishikawa, Y. Nishino, and K. Yamauchi, Sci. Rep. **6**, 24801 (2016).
[22] D. Cocco, G. Bortoletto, R. Sergo, G. Sostero, and I. Cudin, Nucl. Instrum. Methods Phys. Res., Sect. A **616**, 128 (2010).
[23] T. Goto, S. Matsuyama, H. Hayashi, H. Yamaguchi, J. Sonoyama, K. Akiyama, H. Nakamori, Y. Sano, Y. Kohmura, M. Yabashi, T. Ishikawa, and K. Yamauchi, Opt. Express **26**, 17477 (2018).
[24] S. Matsuyama, H. Yamaguchi, T. Inoue, Y. Nishioka, J. Yamada, Y. Sano, Y. Kohmura, M. Yabashi, T. Ishikawa, and K. Yamauchi, Opt. Express **29**, 15604 (2021).
[25] L. Assoufid, N. Brown, D. Crews, J. Sullivan, M. Erdmann, J. Qian, P. Jemian, V. V. Yashchuk, P. Z. Takacs, N. A. Artemiev, D. J. Merthe, W. R. McKinney, F. Siewert, and T. Zeschke, Nucl. Instrum. Methods Phys. Res., Sect. A **710**, 31 (2013).
[26] H. Nakamori and M. Kanaoka, Proc. SPIE. **11492**, 114920A (2020).
[27] O. Hignette, A. K. Freund, and E. Chinchio, Proc. SPIE **3152**, 188 (1997).
[28] J. Sutter, S. Alcock, and K. Sawhney, J. Synchrotron Radiat. **19**, 960 (2012).
[29] T. Goto, S. Matsuyama, H. Nakamori, Y. Sano, Y. Kohmura, M. Yabashi, T. Ishikawa, and K. Yamauchi, Synchrotron Radiat. News **29**, 32 (2016).